Numerical investigation on dynamic ultimate strength of stiffened panels considering real loading scenarios

George Jagite, Fabien Bigot, Quentin Derbanne, Šime Malenica, Hervé Le Sourne, Jérôme De Lauzon, Patrice Cartraud

Numerical investigation on dynamic ultimate strength of stiffened panels considering real loading scenarios

George Jagite [a], Fabien Bigot[b], Quentin Derbanne[b], Šime Malenica[b], Hervé Le Sourne[a], Jérôme de Lauzon[b] and Patrice Cartraud[a]

[a]GeM Institute UMR 6183 CNRS, Ecole Centrale Nantes, Nantes, France; [b]Research Department, Bureau Veritas, Paris, France

In the last 10 years, the importance of whipping on the extreme hull girder loads has received much attention from designers and classification societies. The most common practice to evaluate the ultimate strength of a relatively soft floating structure is to compare the maximum dynamic vertical bending moment after a slamming event with the quasi-static hull girder capacity. Some aspects regarding the current procedure remain unclear, like the capability of the current hydro-elastic methods to accurately predict the extreme dynamic response on the basis of a linear elastic structural model. Moreover, the whipping-induced stresses have a higher frequency than the ordinary wave-induced stresses; hence, the dynamic effects may provide additional strength reserves for the structure and should be investigated. Therefore, the aim of this paper is to investigate the dynamic ultimate strength of stiffened panels considering real loading scenarios, associated with wave loads and whipping response.

KEYWORDS: Dynamic capacity; ultimate strength; strain rate sensitivity; stiffened panels; whipping; ultra large container ship

1. Introduction

Ships and offshore structures are operating in harsh ocean environment and are subjected to different physical phenomena including waves, large ship oscillations, slamming, spray, wind, etc. The collapse of hull girders is the most catastrophic failure event because it almost always generates the complete loss of the structure. Therefore, it is essential to ensure that the structure has sufficient strength to sustain an extreme loading situation.

Until middle of the twentieth century, the design criterion of ship strength was the conventional elastic bending analysis. The first attempt to evaluate the ultimate longitudinal strength of a ship's hull girder was performed by Caldwell in 1965. According to Caldwell (1965), the ultimate strength of a ship is the bending moment which will 'break the back' of the hull girder; and the real margin of safety is the difference between the ultimate bending moment and the maximum bending moment acting on the ship during its lifetime. About 10 years later, Smith (1977) proposed a simple but efficient method to perform progressive collapse analysis on a ship's hull girder in longitudinal bending by dividing the cross-section into small elements composed of stiffeners and their attached plating. In the recent years, with the increase of computer performance and developments of advanced numerical programs, it became possible to apply the finite element method (FEM) to perform collapse analysis of entire ship structures and to analyse the influence of various factors like lateral pressure, thickness reduction due to corrosion, alternate hold loading conditions, etc.

In all the procedures mentioned above, the hull girder ultimate strength analysis is performed under quasi-static conditions, where the maximum total vertical bending moment (VBM) of a ship, obtained from a long-term hydrodynamic analysis, is compared with the maximum VBM that the ship structure can withstand, determined from a progressive collapse analysis

However, relatively 'soft' floating bodies (for example ultra large container ships) may be subjected to transient vibrations after a slamming event, an impulsive hydrodynamic impact between the hull structure and the wave. Such transient vibration of ship structure is called *whipping*. Furthermore, in the last 10 years, the importance of whipping on the extreme hull girder loads has received much attention from researchers, designers and classification societies, especially after the two accidents (i.e. MSC Napoli and MOL Comfort) when the ship hull broke into two pieces after encountering severe damage of the bottom structure. The investigation reports are showing that one possible cause of the accidents is the buckling of the bottom shell plating due to hull girder loads exceeding the hull girder strength (Branch, 2008; ClassNK, 2014).

There are several numerical methods available to analyse the slamming induced whipping response (Bishop and Price, 1979; Domnisoru and Domnisoru, 1998; Tuitman and Malenica, 2009; Derbanne et al., 2010; Seng, 2012). Recently, Andersen and Jensen (2014) performed full-scale measurements on a 9400 TEU container ship showing that, due to the hull girder elasticity, the stress level on a chosen seven wave is magnified by a factor of two, as presented in Figure 1.

Although it is well known that the slamming induced whipping causes a significant increase in the wave loads its consequence on hull girder's collapse is still unclear. The most common practice to evaluate the ultimate strength of a relatively 'soft' floating structure is to compare the maximum

dynamic VBM after a slamming event, which is derived from hydro-elastic calculations, with the quasi-static hull girder capacity. Some aspects regarding the current procedure remain unclear, like the capability of the current hydro-elastic methods to accurately predict the extreme dynamic response on the basis of a linear elastic structural model. Moreover, the whipping-induced stresses have a higher frequency than the ordinary wave-induced stresses; hence, the dynamic effects such as inertia and strain rate effects may provide additional strength reserves for the ship structure and should be investigated.

Several reports on the ultimate strength analysis (Amlashi and Moan, 2008; Shu and Moan, 2012; Matsumoto et al., 2016) showed that, at the point where the ultimate capacity is reached, only the ship's bottom panels experienced plastic deformations. Therefore, the aim of the research work presented in this paper is to analyse the dynamic effects on the ultimate strength of outer bottom stiffened panels subjected to biaxial compression and lateral pressure. Since the remaining structural components are not affected by plastic deformations, the global strain rate effect should be smaller compared to the local one, obtained for the bottom stiffened panel.

A typical stiffened panel, as shown in Figure 2, is composed of a thin plate and several stiffeners. It is important to note that stiffened panels are especially vulnerable to buckling, since the predominantly loads are in-plane. Given the importance, buckling and ultimate strength of stiffened panels have been widely studied in the last century. Considering that the published literature on ultimate strength analysis of stiffened panels is overwhelming, only a short historical review together with some recent contributions are presented here.

The foundations of the linear elastic buckling theory for an ideal axial compressed column have been formulated by Euler (1759). But the pioneering work on large deflection plate theory is attributed to Kirchoff (1850), who discovered the importance of the non-linear terms for large deformations. The final form of the plate differential equations for large deformations were derived by vonKármán (1910). Some recent work in the field of analytic or semi-analytic buckling formulations has been performed by Lin (1985), who proposed a polynomial-type empirical formula that includes two collapse modes: plate-induced and column-like collapse modes. Few years later, Paik and Kim (2002) developed a new method, based on Lin's formula, to predict the ultimate strength of stiffened panels subjected to combined axial load, in-plane bending and lateral pressure. The collapse patterns are classified into six groups, namely overall grillage collapse, yielding at the corners of plating between stiffeners, yielding of the plate-stiffener combination at mid-span, local buckling of stiffener web, lateral-torsional buckling of stiffener and gross yielding. Khedmati et al. (2010) developed closed-form formulations for predicting the ultimate strength of welded stiffened aluminium plates under combined axial in-plane loads and different levels of lateral pressure based on numerical results. Zhang (2016) developed formula for ultimate strength of steel stiffened panels in axial compression using over 100 non-linear finite element analyses.

The finite element method (FEM) was first introduced in 1956 by Turner (1956), but only about 20 years later the FEM was extensively used for the analysis of stiffened plates and marine structures by Soreide et al. (1978). Nowadays, it is a normal practice in structural engineering to perform non-linear finite element analysis to assess the structural capacity of stiffened panels. Therefore, in order to obtain accurate results, several papers have been written to develop some useful insights on non-linear finite element method application for ultimate limit state assessment of plate elements (Paik and Seo, 2009a, 2009b; Zhang and Jiang, 2014)

Though many experiments and numerical analyses to estimate the ultimate strength of stiffened panels have been reported, relatively little work has addressed the dynamic collapse of stiffened panels due to whipping. Jiang et al. (2012) performed dynamic buckling analyses to investigate the influence of various factors on the ultimate strength of ship structures subjected to whipping. They observed an increase of the buckling stress when the stiffened panels are subjected to the dynamic scenarios. Since the cross-sectional area remains constant, this can be interpreted as an increase of the critical buckling load, which represents the ultimate strength of the structure, and we consider that this methodology used to determine the dynamic ultimate capacity of the stiffened panel seems inconsistent. To the authors' knowledge, there is no comprehensive study of the dynamic effects on the ultimate strength of stiffened panels. Therefore, this paper proposes a new definition of the dynamic ultimate capacity, and presents systematic non-linear finite element analyses of the dynamic effects, i.e. strain rate and inertia, on the ultimate strength of 16 stiffened panels subjected to bi-axial compression and lateral pressure. First, the quasi-static ultimate strength is calculated for each panel. Finally, the dynamic load factors (the ratio between the dynamic ultimate strength and the quasi-static ultimate strength) are determined for different scenarios, as well as the ratio between the whipping scenario and wave scenario load factors in order to determine how a stiffened panel capacity will be affected by whipping response.

2. Numerical data

2.1. Geometry

The numerical models are based on the bottom plating stiffened panels of 16 different container ships. The spacing between adjacent transverse frames is denoted by *a* and the distance between adjacent longitudinal stiffeners is denoted by *b*.

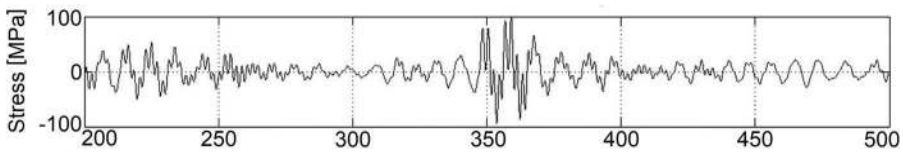

Figure 1. Measured stress on a 9400 TEU container ship.

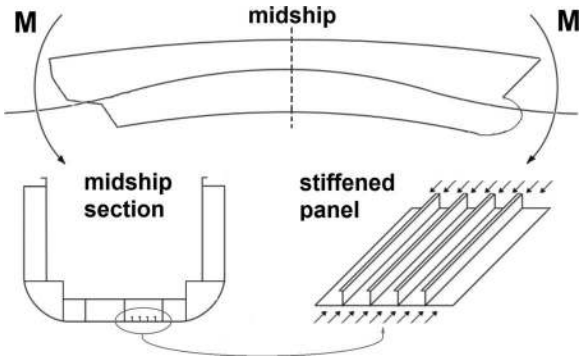

Figure 2. Typical ship structure composition.

To determine the maximum capacity of a stiffened panel, the model is extending over $1/2 + 2 + 1/2$ frame spacings in longitudinal direction and five stiffeners in transverse direction, as indicated in Figure 3.

The dimensions of these panels and the scantlings of the stiffeners are summarised in Table 1. The plate slenderness ratio, denoted by β, is calculated using the Equation (1) where t represents the plate thickness and σ_0 represents the material yield stress. The column slenderness of the beam constituted by the stiffener and its associated plated, denoted by λ, is calculated using Equation (1) where r represents the gyration radius of the stiffener with its attached plating.

$$\beta = \frac{b}{t} \cdot \sqrt{\frac{\sigma_0}{E}}, \quad \lambda = \frac{a}{\pi r} \cdot \sqrt{\frac{\sigma_0}{E}} \tag{1}$$

2.2. Material properties

It is well known that the load rate can induce changes in the material strength properties, and many researchers shown that the plastic flow of some materials is sensitive to strain rate (Manjoine, 1945; Cowper and Symonds, 1957; Rolfe et al., 1974; Jones, 2011; Choung et al., 2013; Paik et al., 2017). The Cowper-Symonds constitutive model, shown in Equation (2), is used extensively in numerical studies.

$$\frac{\sigma_d}{\sigma_0} = 1 + \left(\frac{\dot{\varepsilon}}{C}\right)^{1/q} \tag{2}$$

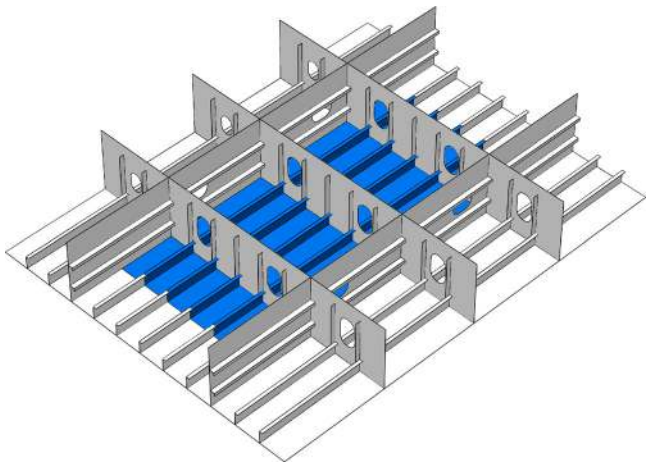

Figure 3. Double bottom structure, extension of the stiffened panel (colored).

Paik et al. (2017) developed a new test database of the mechanical properties of materials for marine applications, including mild steel and high tensile steel. The test database covers strain rates between 10^{-3} and $10^{2}\,s^{-1}$, and temperatures between room temperature, low temperature and cryogenic temperature. The new experimental results for the dynamic yield stress ratio are in very good agreement with the Cowper-Symonds constitutive equation if the constants proposed by Paik and Chung (1999) and Jones (2011) are used. It should be noted that in the tests by Paik et al. (2017) the static yield stress was determined for a strain rate of $10^{-3}\,s^{-1}$, which does not correspond with the recommendations of international standards. According to the classification societies rules (Bureau Veritas, 2018; Det Norske Veritas, 2018), for the determination of the upper yield stress, R_{eH}, the test shall be carried out with an elastic stress rate between 6 and 60 Mpa s^{-1}. On the other hand, in order to minimise the measurement uncertainty, ISO E (2009) proposed a different method to be used when the strain rate sensitive parameters are analysed. For determination of the upper yield stress, R_{eH}, the strain rate shall be kept as constant as possible, between 7×10^{-5} and $2.5 \times 10^{-4}\,s^{-1}$. Figure 4 summarises the experimental results reported by several researchers for the dynamic yield stress ratio of the high tensile steel.

In the numerical analysis, the material of the stiffened panels is high tensile steel (AH32 and AH36) with a Young's modulus of 205.8 Gpa, a Poisson ratio of 0.3 and a yield stress of 315 MPa, and 355 MPa, respectively. Firstly, for the quasi-static analysis, it is defined as an elastic-plastic material including strain hardening with a slope of 1/1000. Finally, in order to analyse the strain rate effect on the dynamic ultimate strength the following constants: C=3200, q=5 were used for the Cowper-Symonds constitutive material model, presented in Equation (2). It is important to notice that according to this model, the flow stress is already increased by 3% at strain rates as low as $10^{-4}\,s^{-1}$, i.e. strain rates that are reached during 'quasi-static' experiments. The effect of this 'inconsistency' on the estimation of the panels' capacity will be discussed later in this paper.

2.3. Load cases

A systematic non-linear finite element analysis has been carried out to study the dynamic effects on the ultimate strength of stiffened panels. For each panel, six load cases of combined compressive longitudinal stress σ_x and transverse stress σ_y are defined. Table 2 summarises all load cases applied to the panel. For each load case, four different levels of lateral pressure are applied: 0.0, 0.1, 0.2 and 0.3 MPa, respectively. The stress ratio, denoted as SR, is defined as the ratio between the axial stress and the sum of axial and transversal stresses.

2.4. Boundary conditions

The choice of the boundary conditions is crucial for the accuracy of the numerical results. Therefore, in the analysis of the ultimate capacity of a stiffened panel, the following boundary conditions are adopted.

Table 1. Geometric characteristics of the stiffened panels considered in the present study.

No.	Name	Span [mm]	Spacing [mm]	t [mm]	Stiffener [mm]	Material	β	λ
1	al841t225	3264	841	22.5	L400x100x11.5/16	AH32	1.462	0.320
2	tb840t20	3250	840	20.0	T400x150x11/18	AH32	1.369	0.267
3	tb840t27	3250	840	27.0	T425x150x11/18	AH32	1.217	0.269
4	ia840t215	3250	840	21.5	L350x100x12/17	AH32	1.776	0.359
5	ia840t185	3250	840	18.5	L350x100x12/17	AH32	1.529	0.346
6	tb840t24	3250	840	24.0	T400x150x11/18	AH32	1.643	0.278
7	fb910t26	1625	910	26	FB225x21	AH32	1.369	0.371
8	ia840t145	3200	840	14.5	L250x90x12/16	AH32	2.266	0.476
9	ia860t13	3160	860	13	L250x90x10/15	AH32	2.588	0.463
10	ia871t155	3150	871	15.5	L300x90x11/16	AH32	2.198	0.397
11	ia875t16	3300	875	16	L300x90x11/16	AH32	2.139	0.420
12	ia890t20	3150	890	20	L350x100x12/17	AH32	1.740	0.347
13	ia910t22	2100	910	22	L250x90x10/15	AH32	1.618	0.296
14	tb840t24b	4200	840	24	T400x150x11.5/25	AH36	1.453	0.351
15	ia732t28	2100	732	28	L250x90x12/16	AH36	1.085	0.376
16	bb905t18	3445	905	18	HP260x11	AH36	2.088	0.678

The primary supporting members (i.e. web frames) are idealised and modelled by boundary conditions. At the intersection lines between the plate and the primary supporting members, the translations on Z-axis are fixed. Also, equations are applied at the intersection between stiffener webs and primary supporting members in order to constrain them to remain vertical.

In Figure 5, the constraints imposed on the boundaries of the stiffened panel are presented. Where UX, UY and UZ denotes the translations along X, Y and Z axes. Similar, RX, RY and RZ denotes the rotations around X, Y and Z axes. Finally, the nodes on CD are constrained by equations to follow the same translation on X-axis as node C. Similar constraints are imposed for the nodes on AD to follow the same translation on Y-axis as node A. Thus, the loads will be applied as concentrated forces on nodes A and C to generate various in-plane bi-axial loads.

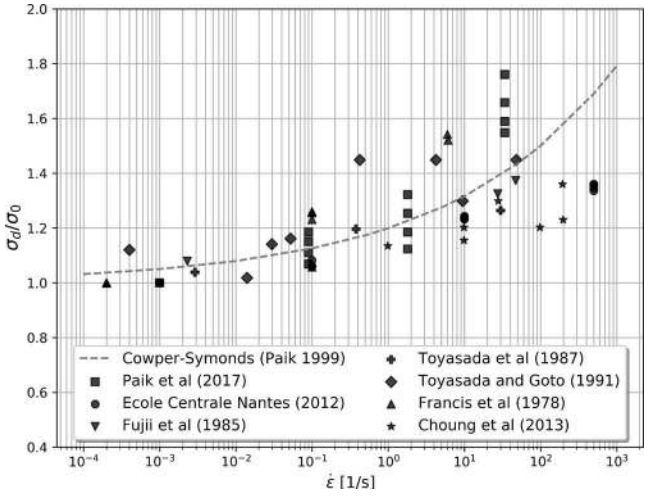

Figure 4. Dynamic yield stress ratio of high tensile steel.

Table 2. Load cases.

Load case	Name	σ_x	σ_y	SR
1	a1	1.0	0.0	1.0
2	a09t01	0.9	0.1	0.9
3	a07t03	0.7	0.3	0.7
4	a05t05	0.5	0.5	0.5
5	a03t07	0.3	0.7	0.3
6	t1	0.0	1.0	0.0

3. Non-linear finite element analyses

Finite element analyses using the computer code ABAQUS (2017) were employed in this study, in which both material and geometric nonlinearities are taken into account. In order to determine the quasi-static capacity, i.e. without any dynamic effects taken into account, the arc-length method is used. This method allows the load to be automatically increased until the ultimate capacity is reached and automatically decreased during the collapse process. If the panel is subjected to lateral pressure and combined in-plane loads then the loads are applied in two consecutive steps. In the first step the lateral pressure is applied and kept constant over the second step when the bi-axial compression is applied.

In the arc-length procedure, the load proportionally factor (LPF) represents one additional degree of freedom in the analysis, therefore it is not possible to use this procedure when analysing the dynamic effects. A dynamic solver must be used for the analysis of strain rate and inertia effect. Thus, the applied loads are defined as a function of time, using a half-sine loading function described by Equation (3), where T represents the period of the load and CF is the amplitude of the load.

$$f(t) = CF \cdot \sin\left(\frac{2\pi}{T} \cdot t\right) \tag{3}$$

Two different scenarios are considered to study the influence of the load period on the panel capacity:

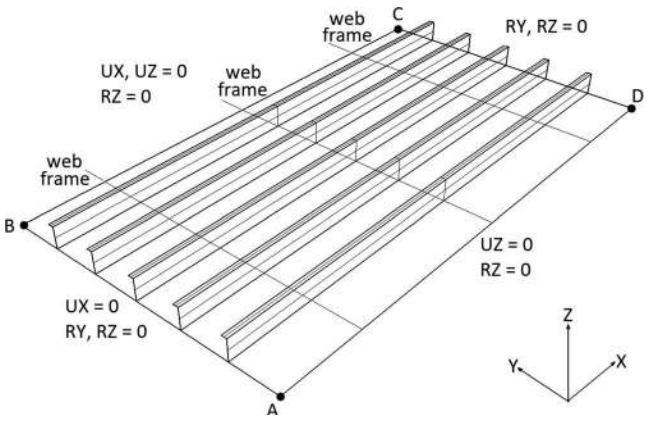

Figure 5. Illustration where the boundary conditions are applied.

- *wave* period scenario, with T=8s
- *whipping* period scenario, with T=1.6s

It should also be mentioned that, at the scale of the entire ship, whipping is not a load but the structural response to a impulsive load. However, in the case of a stiffened panel whipping will be considered as a periodic load imposed by the surrounding structure.

Similar loading scenarios, associated with whipping, are considered by Jiang et al. (2012) to analyse the ultimate capacity of a stiffened panel under uniform axial loads. In the study by Jiang et al., the applied load in the non-linear dynamic analysis was defined as the quasi-static capacity CF_0 multiplied by a factor of 1.2. By scaling the quasi-static capacity by a factor of 1.2, they created a load scenario in which the panel collapsed, and they observed that during the dynamic collapse the applied load gets higher than the panel static capacity. In their work, the critical buckling load represents the applied load, $f(t_{ib})$, at the instant: t_{ib} when the axial displacement started to accelerate rapidly. This time point is defined as 'initiation of buckling'. Since the definition based on the rapid acceleration of axial displacement is quite arbitrary and interpretive, a new definition for the 'initiation of buckling' point is proposed in this paper. Therefore, the failure point of a structure subjected to a load equal to $1.2 \cdot CF_0$ is determined as the point where the slope of the axial displacement vs. time curve is ten times bigger than the initial slope.

According to Jiang et al., the definition of the dynamic capacity (i.e. the critical buckling load) and of the capacity increase is thus as follows:

$$f_{d_{ib}} = \frac{f(t_{ib})}{CF_0} = 1.2 \cdot \sin\left(\frac{2\pi}{T} \cdot t_{ib}\right) \tag{4}$$

$$\overline{f_{d_{ib}}} = 1.2 \cdot \sin\left(\frac{2\pi}{T} \cdot t_{ib}\right) - 1 \tag{5}$$

We consider that this is not a proper definition of the panel dynamic capacity. Indeed, this increased load was reached only during the panel collapse, it is a load level that the panel cannot sustain without collapsing and thus it is of very limited interest for the designer. In this work, we consider that the proper definition of the dynamic capacity is the maximum load that can be applied on the panel without a panel collapse. Therefore, in order to determine the maximum capacity of a stiffened panel, an iterative procedure is employed in this study. Starting from $CF = CF_0$, the amplitude of the load (CF) is increased until the panel fails. The panel dynamic capacity is $CF_{\max}$: the maximum value of CF that the panel can withstand. Since we are interested in the modification of the panel capacity, we define the dynamic load factor f_d as follows:

$$f_d = \frac{CF_{\max}}{CF_0}, \quad \overline{f_d} = \frac{CF_{\max} - CF_0}{CF_0} \tag{6}$$

Moreover, for the comparison of the dynamic load factors obtained in the whipping period and wave period scenarios, we introduce the following ratio:

$$f_{WWR} = \frac{f_{d_{whipping}}}{f_{d_{wave}}}, \quad \overline{f_{WWR}} = \frac{f_{d_{whipping}} - f_{d_{wave}}}{f_{d_{wave}}} \tag{7}$$

In a static simulation, the maximum load is clearly defined, since no static equilibrium can be found when this load is exceeded. However in a dynamic simulation the load can theoretically be arbitrarily increased, the excess of load leading to an acceleration of the structure associated with very high distortion. In this work, the panel was considered has collapsed when the structural deformations become very large, with a rapid reduction in stiffness and the loss of structural stability.

3.1. Mesh sensitivity study results

It is essential to quantify the uncertainties in the numerical model, and thus a mesh convergence study is carried out. Table 3 summarises the average mesh size and number of elements on the plate (between stiffeners), on the stiffener web and on the stiffener flange. The aspect ratio of each element was kept within the range 1:1 to 1:2 (Figure 6).

The results of the sensitivity study on mesh sizes, obtained for model *ia841t225*, are presented in Table 4, where the relative difference is computed with regard to medium mesh size.

Judging from these results, the effect of mesh size over the dynamic load factor is negligible. However, there is a small influence over the quasi-static ultimate capacity, therefore in the following analyses the FE model with medium mesh size is used.

3.2. Geometric initial imperfections

A typical steel structure is usually fabricated by flame cutting and welding, and thus initial imperfections may appear and will reduce the structural capacity. These initial imperfections may be classified in initial distortions and residual stresses. Only initial imperfections related to initial distortions will be considered in this study. Several researchers reported on the importance of the geometric initial imperfections for buckling and ultimate strength analysis. According to Paik (2018), the initial imperfections shape in a numerical analysis can be defined as the fundamental buckling mode for each case of biaxial compression or only for pure longitudinal compression.

An alternative method to the buckling analysis is to define the shape of initial imperfections is the use of analytical expressions and the nodal translation approach (Paik, 2018). Therefore, the number of half-waves in longitudinal direction, denoted as n_{hw}, for a plate subjected to biaxial compression is determined as the smallest integer value that satisfies the Equation (8).

$$\frac{(n_{hw}^2/a^2 + 1/b^2)^2}{n_{hw}^2/a^2 + c/b^2} \leq \frac{[(n_{hw}+1)^2/a^2 + 1/b^2]^2}{(n_{hw}+1)^2/a^2 + c/b^2} \tag{8}$$

Table 3. Mesh density.

Mesh	Elements on span	Elements on spacing	Elements on stiffener height	Elements on stiffener flange
coarse	16	4	2	1
medium	32	8	4	1
fine	32	12	6	1

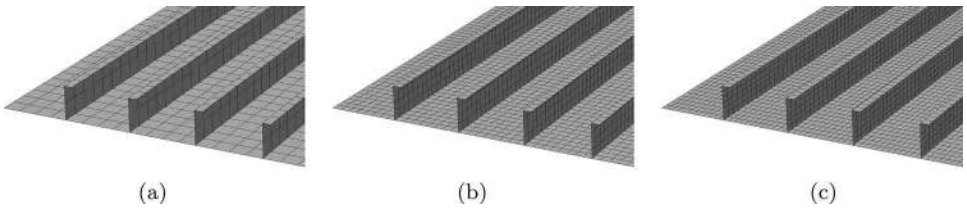

Figure 6. Mesh density (a) coarse mesh (b) medium mesh (c) fine mesh.

where c represents the ratio between the transverse compression σ_y and the longitudinal compression σ_x.

After choosing the shape of the initial geometric imperfections, the next step is to define the maximum amplitude of the initial imperfections. In the current industry practice, an average magnitude for the initial imperfections is usually considered; assuming that the maximum amplitude is a function only of the distance between stiffeners, as shown in Equation (9).

$$w_{pl} = 0.005b \tag{9}$$

Smith et al. (1988) proposed three different levels for the maximum amplitude of the initial geometrical imperfections, as a function of plate slenderness ratio, plate thickness and a coefficient, denoted as c_A, obtained from statistical analysis, as shown in Equation (10).

$$w_{pl} = c_A \beta^2 t \quad \text{and} \quad c_A = \begin{cases} 0.025 & \text{for a slight level} \\ 0.100 & \text{for an average level} \\ 0.300 & \text{for a severe level} \end{cases} \tag{10}$$

A sensitivity study regarding the shape and amplitude of the initial geometric imperfections is performed, and the results are summarised in Table 5 for a stiffened panel (model *tb840t20*) subjected to axial compression and lateral pressure.

The numerical results are showing that the quasi-static ultimate strength is decreasing when the initial imperfections amplitude increases. Also, the dynamic load factors for wave scenario and whipping scenario are proportionally increased with the increase of the initial imperfections amplitude. However, the ratio between the dynamic load factors for whipping and wave scenarios is slightly influenced by the initial imperfections amplitude. Therefore, in the current study the initial imperfections are generated as a combination of:

- local imperfection obtained from a linear buckling analysis. The fundamental buckling mode is retained and scaled so that the deflection of the plate is equal to 1/200 of the stiffeners spacing. Figure 7(a) shows the local imperfection with a 250 magnification factor.
- global imperfection defined analytically, corresponding to column buckling of the stiffeners and their associated plate, with a deflection equal to 1/1000 of the stiffeners span. Figure 7(b) shows the global imperfection magnified with a factor of 100.
- global imperfection defined analytically, corresponding to torsional buckling of the stiffeners, with a deflection equal to 1/1000 of the stiffeners span. Figure 7(c) shows the global imperfection magnified with a factor of 100.

Table 4. Mesh sensitivity results.

Mesh	CF_0 [MN]	diff [%]	$\overline{f_{d\,wave}}$ [%]
Coarse	43.133	1.95	4.6
Medium	42.276	-	4.5
Fine	42.143	−0.31	4.5

4. Results and discussions

Prior to the non-linear dynamic analyses, the first step was to analyse the quasi-static collapse behaviour of the stiffened panels under combined in-plane compression and lateral pressure. The typical deformed shapes are presented in Figure 8, showing that the panel failed due to plastic deformations of the attached plate.

4.1. Inertia effect

One purpose of this study was to investigate the influence of the inertial effect. To this effect, in a first step the strain rate effect was excluded from the analysis by using a simple bi-linear plasticity model. The numerical results are indicating that the inertial effect on the ultimate strength of a stiffened panel is negligible for a load period varying from 1.6 to 16 s. On the other hand, if the duration of the dynamic loading applied to the stiffened panel is very small, the inertia effect will slightly increase the panel's capacity, as shown in Figure 9. For a load with a period of 0.2 s the dynamic ultimate strength is increased with 1%.

4.2. Strain rate effect

After analysing the inertial effect on the ultimate strength, the next step is to study the influence of the strain rate on the ultimate capacity using a series of dynamic analyses. Therefore, starting from the quasi-static capacity of the stiffened panels, the dynamic capacity for each panel was determined by increasing the load amplitude until the panel fails. A typical example

Table 5. Effect of the initial imperfections amplitude on the quasi-static ultimate capacity and the dynamic capacity for wave and whipping scenarios.

Initial imperf	prs [MPa]	CF_0 [MN]	$\overline{f_{d\,wave}}$[%]	$\overline{f_{d\,whipping}}$[%]	$\overline{f_{WWR}}$[%]
Best	0.0	38.77	4.3	5.8	1.4
Practice	0.2	36.01	5.3	7.1	1.7
Slight level	0.0	42.04	4.0	5.4	1.3
(Smith)	0.2	38.95	5.1	6.9	1.7
Average level	0.0	39.12	4.2	5.6	1.3
(Smith)	0.2	36.34	5.2	7.0	1.7
Severe level	0.0	35.17	5.0	6.9	1.8
(Smith)	0.2	32.90	5.8	7.8	1.8

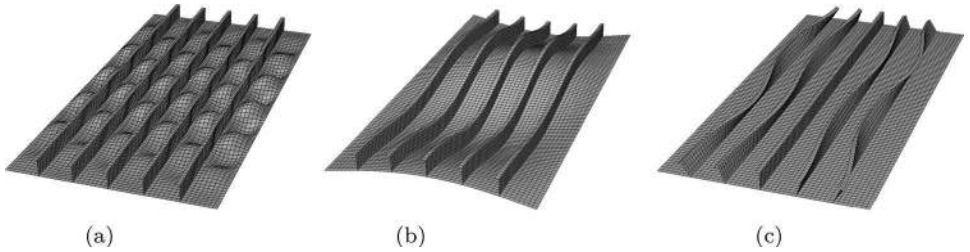

Figure 7. Initial geometric imperfections (a) local imperf. (b) column buckling imperf. (c) torsional buckling imperf.

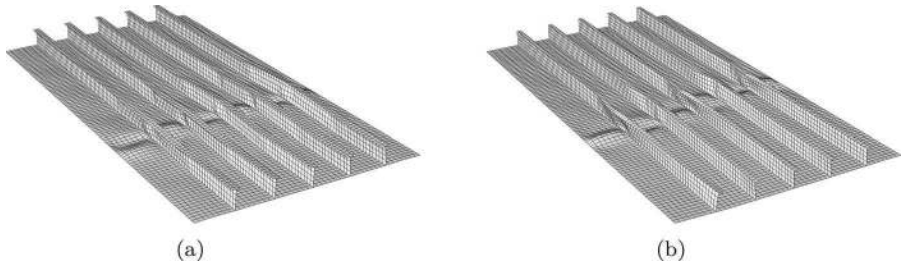

Figure 8. Typical deformed shape (a) model 2, SR=1, prs=0.3 MPa (b) model 5, SR=1, prs=0.0 MPa.

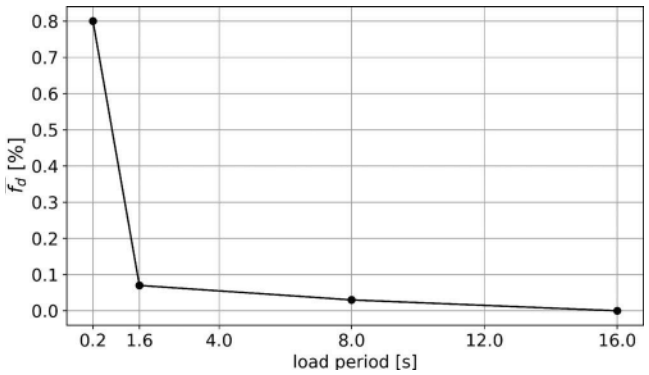

Figure 9. Dynamic load factor vs. load period.

for the variation of the dynamic load factor under all scenarios and different load combinations is presented in Figure 10. Similar results were obtained for all other models analysed in this research work.

By examining the results from the non-linear dynamic analyses it can be concluded that the dynamic load factor increases when the load period decreases and also when the applied lateral pressure increases. Also, it can be concluded that the highest values of the dynamic load factor are obtained for pure axial compression, *SR*=1. Therefore, in the following comparison only the worst load case will be considered for each stiffened panel.

In order to show the importance of correctly defining the dynamic ultimate strength, a comparison between the dynamic load factors obtained for the whipping period scenario using Jiang's definition (Equation (5)) on one hand, and using our new definition (Equation (7)) on the other hand was made and it is presented hereafter.

The numerical results presented in Table 6, when stiffened panel's structure is subjected to a load equal to $1.2 \cdot CF_0$, are showing that the dynamic effects will increase the dynamic capacity at the initiation of buckling from 8.8% to 10.5%. However, when the dynamic ultimate strength is correctly evaluated with our new definition, the dynamic capacity increase is only 4.8% to 7.2%.

It can be observed that the whipping dynamic capacity increase with our definition is systematically lower than the

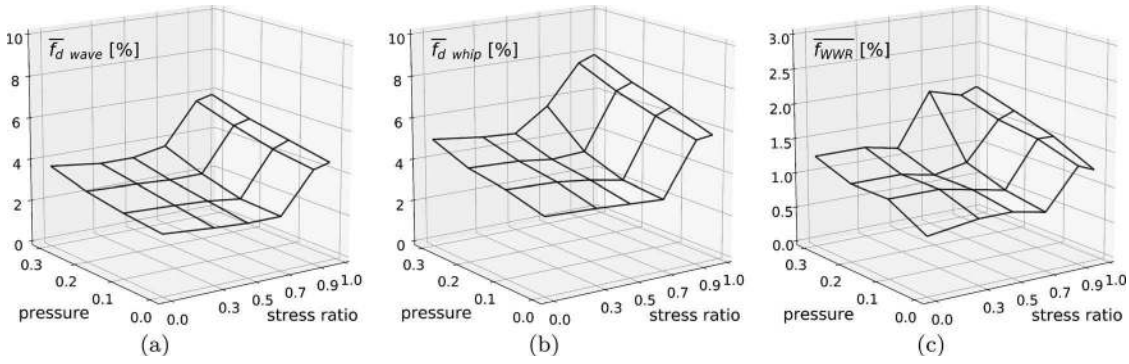

Figure 10. Dynamic load factor distribution for all scenarios (a) wave scenario (b) whipping scenario (c) whipping-wave ratio.

Table 6. Comparison of the different definitions of the dynamic capacity increase, for whipping scenario.

Model	CF_0	t_{ib}	$\overline{f_{dib}}$	$\overline{f_{dwhip}}$	model	CF_0	t_{ib}	$\overline{f_{dib}}$	$\overline{f_{dwhip}}$
ia840t185	34.10	0.292	9.4	5.6	ia732t28	50.43	0.298	10.5	7.2
ia840t215	40.04	0.295	9.9	5.8	ia860t13	19.81	0.294	9.8	5.2
ia841t225	42.28	0.295	9.9	6.1	ia871t155	26.20	0.290	9.0	5.2
fb910t26	48.75	0.294	9.8	6.1	ia875t16	27.37	0.289	8.8	5.0
ia840t145	23.80	0.289	8.8	4.8	ia890t20	37.50	0.292	9.4	5.4
ia910t22	36.67	0.297	10.3	5.8	tb840t24	46.75	0.295	9.9	6.2
tb840t20	38.78	0.294	9.8	5.7	tb840t24b	53.68	0.298	10.5	6.0
tb840t27	52.77	0.296	10.1	6.5	bb905t18	32.33	0.290	9.0	5.0

one with Jiang's definition. The corollary is that none of the panels can actually withstand the load defined by Jiang's definition without collapsing. This confirms the need for the new definition.

The results of the dynamic analyses for all panels under axial compression are summarized in Table 7. In Figure 11, we show a comparison between the dynamic load factors obtained with our new definition for wave and whipping period scenarios, together with those obtained with Jiang's definition for whipping period.

From the results shown in Table 7 and Figure 11, we can observe that the effect of strain rate is already existent for the wave period scenarios. This is not surprising since as mentioned in Section 2.2, with the considered Cowper-Symonds model it was expected that some strain rate effects are observed in the response to 'quasi-static' loads. However, this is in contradiction with the long established industry practice to consider the wave periods as quasi-static.

We believe that two different interpretations can be made of this finding. The first interpretation is that this apparent increased capacity in the response to the wave scenario is an artefact of the considered strain rate model, and of the inconsistency mentioned in Section 2.2. As a consequence, the industry practice would be confirmed, and we should change the Cowper-Symonds model, or define another equation that would give no increase for strain rates below $10^{-3}\,s^{-1}$ and thus no (or negligible) increased capacity for wave period scenarios.

Figure 12 shows the dependency of the dynamic load factor with the maximum local strain rate obtained during the analysis. The numerical results are indicating that a wave scenario produces strain rates up to $10^{-2}\,s^{-1}$. On the other hand, during the whipping period scenario the strain rates are about one order of magnitude higher, in a range from about $10^{-2}\,s^{-1}$ to $10^{-1}\,s^{-1}$.

These results show that the part of the Cowper-Symonds constitutive model involved in the wave period scenarios and also in the whipping period scenarios is the part where the validity of the model is questionable, as discussed in Section 2.2. As shown in Figure 13, the Cowper-Symonds curve is not very consistent with the results of the 'quasi-static yield stress experiments'. By construction, the curve is significantly above the experimental data in this range of strain rates. The only exceptions are a few experimental points for which it is not clear how the 'quasi-static' yield stress used to normalise the data has been defined, since these points are far above 1.0 at very low strain rates.

The second possible interpretation of the apparent increased capacity for the wave period scenarios is that the strain rate model with the Cowper-Symonds parameters proposed by Paik is correct, and thus this increased capacity is real, although the industry practice is to neglect it. In this case it would not be consistent to consider the whole capacity increase for whipping scenarios, and the logic is to only retain the whipping increase relative to the wave one: $\overline{f_{WWR}}$.

It is beyond the scope of this work to determine which interpretation is correct, and also to propose an alternative strain rate model or set of coefficients. Therefore, we decided to keep for now the parameters given by Paik and to consider the relative increase $\overline{f_{WWR}}$ as the proper estimator of the increased capacity that could be used when designing or checking the structure against whipping. In this case, the increment of the stiffened panel capacity under whipping scenario is between 1.6% and 2.1% when a pressure is applied and between 1.2% and 1.7% without pressure, as shown in Figure 14.

Table 7. Comparison of the different definitions of the dynamic capacity increase, for whipping scenario.

Model	prs	$\overline{f_{dlong}}$	$\overline{f_{dwave}}$	$\overline{f_{dwhip}}$	$\overline{f_{WWR}}$	model	prs	$\overline{f_{dlong}}$	$\overline{f_{dwave}}$	$\overline{f_{dwhip}}$	$\overline{f_{WWR}}$
al840t185	0.0	3.7	4.2	5.6	1.3	ia732t28	0.0	4.8	5.4	7.2	1.7
	0.25	4.8	5.4	7.2	1.7		0.3	5.4	6.1	8.3	2.1
al840t215	0.0	3.9	4.5	5.8	1.2	ia860t13	0.0	3.4	3.8	5.2	1.3
	0.3	5.3	5.9	7.9	1.9		0.1	4.4	4.9	6.8	1.8
al841t225	0.0	4.0	4.6	6.1	1.4	ia871t155	0.0	3.4	3.8	5.2	1.3
	0.3	5.2	5.8	7.9	2.0		0.1	3.8	4.3	6.0	1.6
fb910t26	0.0	4.0	4.5	6.1	1.5	ia875t16	0.0	3.4	3.8	5.0	1.2
	0.3	4.6	5.2	7.0	1.7		0.1	4.0	4.3	6.0	1.6
ia840t145	0.0	3.1	3.5	4.8	1.3	ia890t20	0.0	3.6	4.0	5.4	1.3
	0.3	4.0	4.3	6.0	1.6		0.2	4.5	5.0	6.8	1.7
ia910t22	0.0	4.0	4.4	5.8	1.3	tb840t24	0.0	4.1	4.6	6.2	1.5
	0.3	4.9	5.5	7.4	1.8		0.3	5.2	5.9	7.8	1.8
tb840t20	0.0	3.9	4.3	5.7	1.3	tb840t24b	0.0	4.0	4.6	6.0	1.3
	0.3	5.1	5.6	7.6	1.9		0.3	5.2	5.9	8.1	2.1
tb840t27	0.0	4.2	4.8	6.5	1.6	bb905t18	0.0	3.2	3.6	5.0	1.4
	0.3	5.2	5.9	8.0	2.0		0.2	4.4	4.9	6.7	1.7

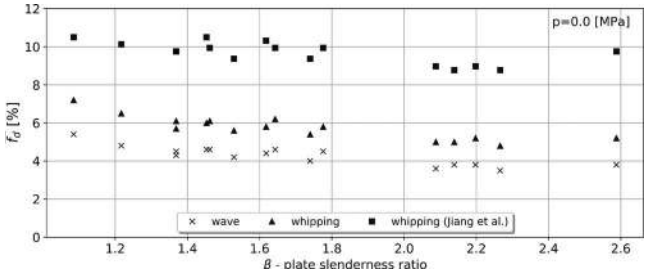

Figure 11. Dynamic load factor for all panels under pure in-plane axial compression vs their plate slenderness ratio.

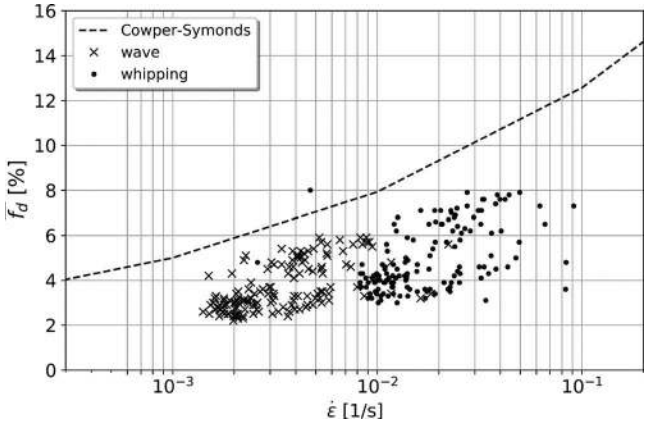

Figure 12. Dynamic load factor vs. strain rate.

5. Real loading scenarios

The objective of this research work is to analyse the influence of the dynamic effects on the ultimate strength of stiffened panels. In the previous chapter, it was shown that the inertial effect is negligible for a load period between 1.6 s and 16 s. Also, by using simplified loading scenarios, it was demonstrated that the strain rate effect is already existent in the wave loads, and if the panel is subjected to high frequency transient loads the strain rate effect will slightly increase the ultimate capacity. In a real environment, the high frequency transient loads (whipping) are always combined with low frequency (wave) loads. Therefore, it can be anticipated that the strain rates obtained

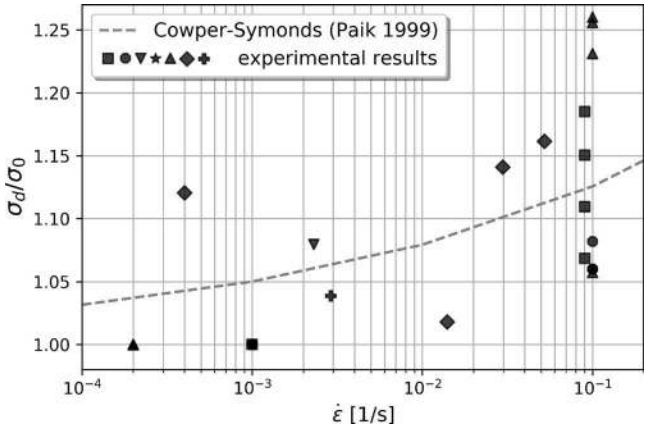

Figure 13. Dynamic yield stress ratio for high tensile steel (extracted from Figure 4).

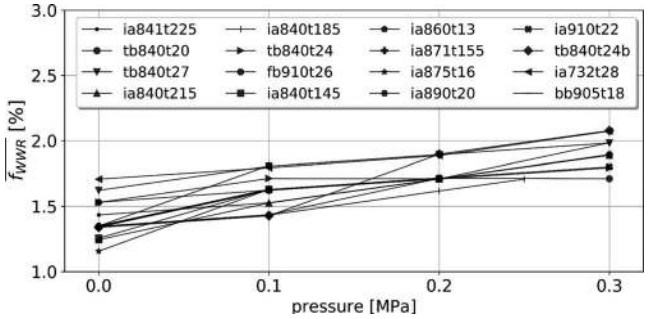

Figure 14. Dynamic load ratio between whipping and wave scenarios vs. lateral pressure.

in the simplified 'whipping period' scenarios in which 100% of the load was varying at the whipping frequencies were overestimated, and so was the strain rate effect on the panels capacity. In order to obtain a better estimation of the actual panel capacity increase in the context of whipping, a hydroelastic analysis was performed on an ultra large container ship to determine more realistic whipping loading scenarios. The principal characteristics of the ULCS used in this study are presented in Table 8.

The software HOMER, developed at Bureau Veritas, was used to perform the hydro-elastic coupling between a 3D hydrodynamic solver and a beam model based on non-uniform Timoshenko beam theory for the hull girder. The hydro-elastic model is based on the generalised modes approach; the complete procedure for the fully coupled seakeeping, slamming and whipping analysis can be found in Derbanne et al. (2010). First the mode shapes for several elastic modes are calculated and used later to extend the motion/deformation modes in the hydrodynamic solver. After solving the hydrodynamic boundary value problems, the resulting pressure is integrated over the wetted surface in order to obtain the hydrodynamic forces, so that the coupled dynamic Equation (11) can be written.

$$\{-\omega_e^2([m]+[A]) - i\omega_e[B]+[k]+[C]\}\{\xi\} = \{F^{DI}\} \quad (11)$$

The solution of Equation (11) gives the motion amplitudes and phase angles for six rigid body modes and a certain number of elastic modes. The non-linear time domain model uses the frequency domain hydrodynamic solution and transfers it to time domain using the inverse Fourier transform. In this way the following time domain motion Equation (12) is

Table 8. Geometrical characteristics of ULCS.

Length overall	340 m	Breadth moulded	42.8 m
Draught	14.8 m	Capacity	8500 TEU
Geometric area of cross-section	6.55 m^2	Position of neutral axis	12 m
Moment of inertia /Gy axis	707.52 m^4	Moment of inertia /Gz axis	1958.22 m^4
Shear centre transversal coordinate	−13.86 m	Warping moment of inertia	186 144.6 m^6
1st vertical mode frequency	0.492 Hz	2nd vertical mode frequency	1.036 Hz

obtained:

$$([m] + [A^{\infty}])\{\ddot{\xi}(t)\} + [k]\{\xi(t)\} + \int_0^t [K(t-\tau)]\{\dot{\xi}(\tau)\}\mathrm{d}\tau = \{F^{DI}(t)\} + \{Q(t)\} \quad (12)$$

The time domain calculation will automatically include the linear and non-linear springing. In order to calculate the slamming induced whipping response, the slamming forces are calculated using the Generalized Wagner Model, and are added to the force vector Q(t) of Equation (12).

The objective of the hydro-elastic analysis is to estimate the levels of the still water, wave frequency and whipping frequency components of the vertical bending moment, and to determine the load time series which will be used to define real loading scenarios on the stiffened panels. The time domain simulations are performed on irregular waves using an increased design sea state (IDSS). Additional details about the IDSS methodology can be found in Derbanne et al. (2012). Figure 15 shows a representative time variation of vertical wave bending moment(VWBM) at midship with and without slamming induced whipping.

Based on the load time series several significant time samples are extracted and these loads are applied on the stiffened panel model. During a first loading step, the lateral pressure loads are defined using a smooth step amplitude function. In a second loading step, the axial compression due to vertical wave bending moment (with and without whipping) is applied. For each 'real loading' scenario, shown in Figure 16, the dynamic ultimate strength is computed using the iterative procedure described in Section 3. The results for the *wave* and *wave+whipping* real scenarios are presented in Table 9.

The numerical results presented in Table 9 and Figure 17 are showing that the strain rate effect is already existent in the wave loads, and if the panel is subjected to wave+whipping loads the strain rate will increase. Due to higher strain rate the panel's capacity is increased by 0.4% to 1.3%. In a realistic loading scenario, the low frequency loads are combined with the high frequency loads; and therefore, it can be concluded that the simplified whipping scenario, defined in Section 4, over predicts the increase of dynamic load factors due to whipping.

The whipping-wave dynamic load ratios ($\overline{f_{WWR}}$) obtained for pure axial compression (i.e. without lateral pressure) for the real loading scenarios are compared to the results obtained for simplified scenarios in Figure 18. It can be observed that real loading scenarios lead to a significantly smaller ratio.

6. Conclusion

In this paper, the numerical results of the dynamic collapse analysis for different stiffened panels, extracted from 16 container ships, are presented. Each panel is subjected to in-plane biaxial loads and to water pressure lateral loads. In the first part of the analysis, the quasi-static capacity of these panels was determined. In the second part, the quasi-static capacity was used to define dynamic load time scenarios for two typical periods associated with wave and whipping. A new and proper definition of the panel dynamic ultimate capacity was introduced. By analysing the numerical results, it can be concluded that the inertial effect on the ultimate capacity of stiffened panels is negligible for a periodic load varying from 1.6 to 16

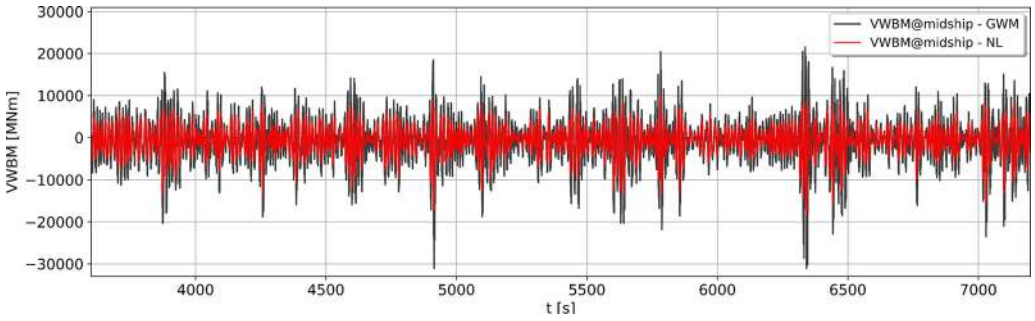

Figure 15. Load time series for VWBM at midship.

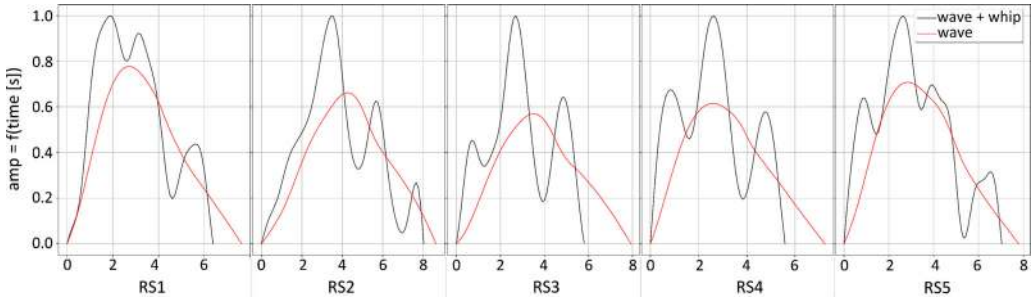

Figure 16. Amplitude functions for real load time series extracted from time-domain hydro elastic analysis.

Table 9. Dynamic load factors [%] variation for real loading scenarios.

Case	prs	RS1		RS2		RS3		RS4		RS5	
		$\overline{f_{dwhip}}$	$\overline{f_{WWR}}$	$\overline{f_{dwhip}}$	$\overline{f_{WWR}}$	$\overline{f_{dwhip}}$	$\overline{f_{WWR}}$	$\overline{f_{dwhip}}$	$\overline{f_{WWR}}$	$\overline{f_{dwhip}}$	$\overline{f_{WWR}}$
ia732t28	0	5.6	0.57	5.8	0.76	5.9	0.86	5.8	0.86	5.9	0.95
	0.3	6.5	0.76	6.7	0.95	7.2	1.32	6.8	1.14	6.8	1.14
ia840t145	0	3.7	0.39	3.8	0.39	4.0	0.58	4.0	0.68	3.9	0.58
	0.15	5.2	0.57	5.3	0.57	5.5	0.76	5.4	0.76	5.6	0.96
ia840t185	0	4.5	0.48	4.6	0.58	5.0	0.86	4.7	0.77	4.7	0.77
	0.25	5.7	0.57	6.0	0.76	6.0	0.76	6.0	0.86	6.1	0.95
ia841t225	0	4.9	0.58	5.0	0.57	5.5	1.05	5.1	0.77	5.1	0.77
	0.3	6.2	0.66	6.5	0.85	6.5	0.85	6.5	1.04	6.6	1.14
ia910t22	0	4.6	0.48	4.7	0.48	4.7	0.48	4.8	0.67	4.9	0.77
	0.3	5.8	0.57	5.9	0.67	6.1	0.76	6.1	0.95	6.2	1.05
ia840t27	0	5.1	0.48	5.3	0.67	5.7	1.05	5.4	0.86	5.4	0.86
	0.3	6.3	0.66	6.5	0.76	7.0	1.23	6.7	1.14	6.8	1.23

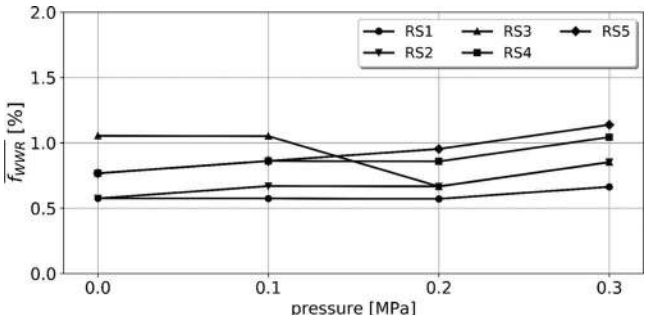

Figure 17. Dynamic load factor ratio between *wave+whipping* and *wave* real scenarios for model *ia910t22*.

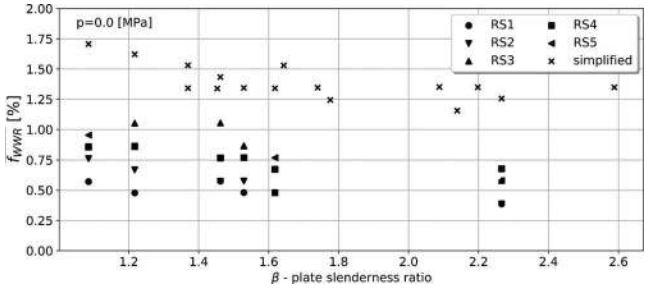

Figure 18. Comparison of whipping-wave load ratio between simplified and real scenarios.

s. On the other hand, the strain rate effect on the material constitutive law has some impact on the panel ultimate strength. With the new consistent definition of the dynamic capacity the capacity increase, originally in a [8.8–10.5%] range, is reduced to [4.8–7.2%].

However, under the hypotheses on the strain rate effect on the material yield stress that have been considered, the increase in ultimate capacity for wave loadings is already in the range of 3.5–6% while the industry practice is to consider no strain rate effect for such loads. The question whether this capacity increase for wave loads is real or is a bias due to the hypotheses is still open, but this result lead us to the conclusion that the capacity increase for whipping period scenarios has to be considered relatively to the increase for the wave period scenarios. When this is taken into account, the stiffened panel capacity increase under simplified whipping period scenario is only 1.2% to 2.1%.

The objective of the last part of the current research work was to compare the strain rate effect on the stiffened panel dynamic capacity under a real loading scenario, obtained from a hydro elastic analysis on a ULCS. The numerical results obtained from non-linear finite element analyses are showing that under a real *wave+whipping* loading scenario the stiffened panel's capacity is increased by 0.4% to a maximum of 1.3% comparing to a real *wave* loading scenario. It shows that simplified scenarios tend to over-predict the increase of the panel's capacity due to whipping.

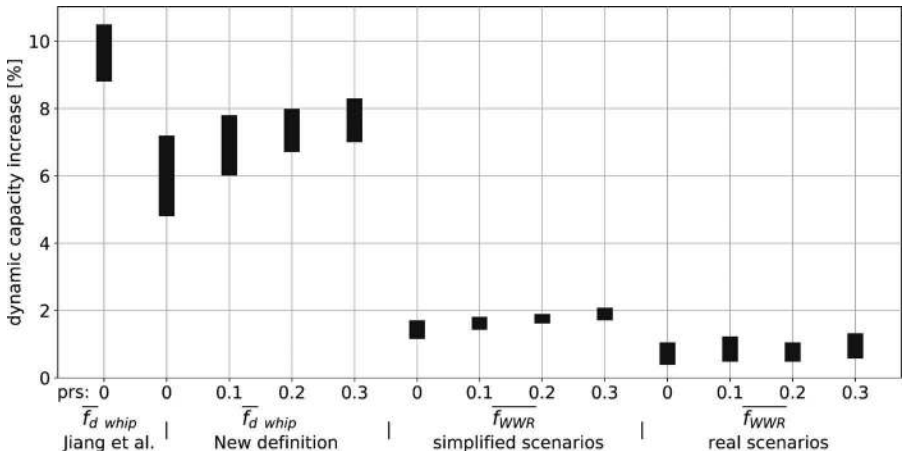

Figure 19. Summary of dynamic capacity increase.

Figure 19 summarises all the results presented in this paper. It shows that by over-increasing the applied load, as per Jiang's definition, the dynamic capacity, interpreted as the critical buckling load, was overestimated. However, using an improved definition, the dynamic load factors are significantly reduced. Furthermore, considering that the wave scenario is accepted as quasi-static, the increase due to whipping is only between 1.2% and 2.1%. Moreover, the use of realistic loading scenarios further reduces the increase of the capacity with a factor of two. Therefore, it seems that the usual assumption that strain rate effect can be neglected in the ultimate strength analysis of ship structure subjected to wave loads can be extended to the analysis of structures subjected to whipping loads.

In addition, according to several reports on the ultimate strength analysis of ULCS (Matsumoto et al., 2016; Fujikubo and Tatsumi, 2017), at the point where the ultimate capacity of the hull girder is reached very few structural members undergo plastic deformations. Since the rest of the structure remains elastic, the strain rate effect on the hull girder ultimate bending strength of ULCS should be smaller than the one of a bottom stiffened panel. Therefore, in a future work, an extended ship model will be used to verify that the strain rate effect on the ultimate hull girder capacity of a container ship under whipping loads is practically negligible.

Nomenclature

a	spacing between transverse frames
b	spacing between longitudinal stiffeners
t	plate thickness
β	plate slenderness ratio
λ	column slenderness ratio
σ_0	static yield stress
σ_d	dynamic yield stress
CF_0	quasi-static ultimate strength
$CF_{\max}$	dynamic ultimate strength
$\frac{f_d}{f_{WWR}}$	dynamic load factor increase rate whipping-wave dynamic load ratio increase rate
$\dot{\varepsilon}$	strain rate
ULCS	ultra large container ship

Acknowledgments

The present research work was undertaken at Ecole Centrale de Nantes, France, as a part of the Ph.D. thesis on the analysis of whipping effects over the hull girder's ultimate strength.

Disclosure statement

No potential conflict of interest was reported by the authors.

Funding

The first author is pleased to acknowledge the funding and support of Bureau Veritas via BV-ECN cooperation.

ORCID

George Jagite http://orcid.org/0000-0001-6479-2498

References

ABAQUS. 2017. Dassault Systemes Simulia Corp, Johnston (RI), USA.

Amlashi HK, Moan T. 2008. Ultimate strength analysis of a bulk carrier hull girder under alternate hold loading condition – a case study: part 1: nonlinear finite element modelling and ultimate hull girder capacity. Marine Struct. 21(4):327–352.

Andersen IMV, Jensen JJ. 2014. Measurements in a container ship of wave-induced hull girder stresses in excess of design values. Marine Struct. 37:54–85.

Bishop RE, Price WG. 1979. Hydroelasticity of ships. Cambridge University Press.

Branch MAI. 2008. Report on the investigation of the structural failure of MSC Napoli, English channel on 18 january 2007. Marine Accident Investigation Branch. Report No: 9/2008.

Bureau Veritas. 2018. Rules on materials and welding for the classification of marine units. Bureau Veritas.

Caldwell J. 1965. Ultimate longitudinal strength. Trans RINA. 107:411–430.

Choung J, Nam W, Lee JY. 2013. Dynamic hardening behaviors of various marine structural steels considering dependencies on strain rate and temperature. Marine Struct. 32:49–67.

ClassNK. 2014. Investigation report on structural safety of large container ships. ClassNK.

Cowper GR, Symonds PS. 1957. Strain-hardening and strain-rate effects in the impact loading of cantilever beams. Brown Univ Providence Ri. Report No: TR-C11-28.

Derbanne Q, Bigot F, de Hauteclocque G. 2012. Comparison of design wave approach and short term approach with increased wave height in the evaluation of whipping induced bending moment. In: ASME 2012 31st International Conference on Ocean, Offshore and Arctic Engineering. American Society of Mechanical Engineers. p. 299–308.

Derbanne Q, Malenica Š, Tuitman J, Bigot F, Chen X. 2010. Validation of the global hydroelastic model for springing & whipping of ships. In: 11th International Symposium on Practical Design of Ships and Other Floating Structures, Rio de Janeiro, p. 331–340.

Det Norske Veritas. 2018. Os-b101 metallic-materials. Det Norske Veritas.

Domnisoru L, Domnisoru D. 1998. The unified analysis of springing and whipping phenomena. Trans R Inst Naval Architect London. 140:19–36.

Euler L. 1759. Sur la force des colonnes. Memoires de L'Academie des Sci et Belles-Lett. 13:252–282.

Fujikubo M, Tatsumi A. 2017. Progressive collapse analysis of a container ship under combined longitudinal bending moment and bottom local loads. In: Proceedings of the 6th international conference on Marine Structures, Lisbon, Portugal. p. 235–242.

ISO E. 2009. 6892-1. metallic materials-tensile testing-part 1: Method of test at room temperature. International Organization for Standardization.

Jiang L, Zhang S, White N. 2012. Nonlinear finite element dynamic collapse analyses of stiffened panels. In: Proceedings of the Sixth International Conference on Hydroelasticity in Marine Technology, Tokyo, Japan, Sept. p. 19–21.

Jones N. 2011. Structural impact. Cambridge university press.

Khedmati MR, Zareei MR, Rigo P. 2010. Empirical formulations for estimation of ultimate strength of continuous stiffened aluminium plates under combined in-plane compression and lateral pressure. Thin-Walled Struct. 48(3):274–289.

Kirchoff G. 1850. Uber das gleichgewicht und die bewegung einer elastischen scheibe. J fur die reine und angewandte Mathematik (Crelle's J). 40:51–88.

Lin Y. 1985. Structural longitudinal ship modelling [dissertation]. Department of Naval Architecture and Ocean Engineering, University of Glasgow Scotland.

Manjoine M. 1945. Influence of rate of strain and temperature on yield stresses of mild steel. J Appl Mech Trans ASME. 12(3): A186.

Matsumoto T, Shigemi T, Kidogawa M, Ishibashi K, Sugimoto K. 2016. Examination of effect of lateral loads on the hull girder ultimate

strength of large container ships. In: ASME 2016 35th International Conference on Ocean, Offshore and Arctic Engineering. American Society of Mechanical Engineers.
Paik JK. 2018. Ultimate limit state design of steel-plated structures. 2nd ed. Wiley.
Paik J, Chung J. 1999. A basic study on static and dynamic crushing behavior of a stiffened tube. KSAE Trans. 1:219–238.
Paik JK, Kim BJ. 2002. Ultimate strength formulations for stiffened panels under combined axial load, in-plane bending and lateral pressure: a benchmark study. Thin-Walled Struct. 40(1):45–83.
Paik JK, Kim KJ, Lee JH, Jung BG, Kim SJ. 2017. Test database of the mechanical properties of mild, high-tensile and stainless steel and aluminium alloy associated with cold temperatures and strain rates. Ships Offshore Struct. 12(sup1):230–256.
Paik JK, Seo JK. 2009a. Nonlinear finite element method models for ultimate strength analysis of steel stiffened-plate structures under combined biaxial compression and lateral pressure actions-part i: plate elements. Thin-Walled Struct. 47(8–9):1008–1017.
Paik JK, Seo JK. 2009b. Nonlinear finite element method models for ultimate strength analysis of steel stiffened-plate structures under combined biaxial compression and lateral pressure actions-part ii: stiffened panels. Thin-Walled Struct. 47(8):998–1007.
Rolfe ST, Rhea DM, Kuzmanovic BO. 1974. Fracture-control guidelines for welded steel ship hulls. Washington: Kansas University Lawrence. Report No: 244.
Seng S. 2012. Slamming and whipping analysis of ships [dissertation]. DTU Mechanical Engineering.
Shu Z, Moan T. 2012. Ultimate hull girder strength of a bulk carrier under combined global and local loads in the hogging and alternate hold loading condition using nonlinear finite element analysis. J Marine Sci Technol. 17(1):94–113.
Smith CS. 1977. Influence of local compressive failure on ultimate longitudinal strength of a ship's hull. Proc Int Sym Practical Design Shipbuilding. 1977:73–79.
Smith CS, Davidson P, Chapman J. 1988. Strength and stiffness of ships'-plating under in-plane compression and tension. R Inst Naval Architect Trans. 130:277–296.
Soreide T, Moan T, Nordsve N. 1978. On the behavior and design of stiffened plates in ultimate limit state. J Ship Res. 22(4):238–244.
Tuitman J, Malenica Š. 2009. Fully coupled seakeeping, slamming, and whipping calculations. Proc Inst Mech Eng Part M: J Eng Maritime Environ. 223(3):439–456.
Turner M. 1956. Stiffness and deflection analysis of complex structures. J Aeronaut Sci. 23(9):805–823.
von Kármán T. 1910. Untersuchungen über knickfestigkeit. In: Mitteilungen über forschungsarbeiten auf dem gebiete des ingenieurwesens insbesondere aus den laboratorien der technischen hochschulen. Springer; p. 1–44.
Zhang S. 2016. A review and study on ultimate strength of steel plates and stiffened panels in axial compression. Ships Offshore Struct. 11 (1):81–91.
Zhang S, Jiang L. 2014. A procedure for non-linear structural collapse analysis. In: ASME 2014 33rd International Conference on Ocean, Offshore and Arctic Engineering. American Society of Mechanical Engineers. p. 19–21.